JOURNAL OF PETROLEUM GEOMECHANICS
(JPG)

Analysis of the stability of open-hole multilateral wells with consideration of intermediate principal stress

Hasan Ghasemzadeh[1*], Erfan Rahimi[1], Mohammad Ali Iranmanesh[1]

1- Civil Engineering Faculty, K. N. Toosi University of Technology | Tehran, Iran

Received: 12 November 2024; Accepted: 24 December 2024

DOI: 10.22107/jpg.2025.488426.1244

Keywords

Multilateral Well, Intermediate Principal Stress, Mogi-Coulomb, Well Stability, Finite Element Method (FEM)

Abstract

Geomechanics is one of the sciences that plays a fundamental role in the production of energy from the earth. Today, this science is widely used in the design and drilling of wells, as well as in reservoir engineering. Safe drilling is an essential parameter in the oil and gas industry. Modern drilling methods, such as multilateral(ML) wells, increase production efficiency. However, drilling such wells is associated with mechanical instability. Those issues depend on the formation strength parameters, in-situ stress, well-direction, pore-pressure, and fluid parameters. The study of stability requires a failure criterion. Hereof, some failure criteria do not consider the role of intermediate principal stress(σ2), which is proven to have a considerable effect on mechanical failure. Our study uses the three-dimensional(3D) finite element method(FEM) to investigate the stability and solid deformation of an ML well that follows the Mohr-Coulomb(MC) and Mogi-Coulomb(Mogi-C) failure criterion to studying of mechanical failure. The results were shown in different graphs such as changes in surface pressure, flow lines around the well and fracture for different borehole pressures using Mogi-C and MC fracture criteria. Our results revealed that the weakest range in these wells is at the junction of branches. Due to the principal stress effects, using the Mogi-C criterion is more safe and closer to reality. The results demonstrate an approximate 30% reduction in predicted failure points under pressures exceeding 30 MPa when employing the Mogi-C criterion, with predicted failures decreasing from approximately 15% to 5% at 35 MPa.

1. Introduction

The stability of open-hole ML wells is a critical concern in the oil and gas industry, particularly as drilling technologies evolve to enhance production efficiency. ML wells, characterized by multiple lateral branches extending from a parent well, provide significant advantages regarding reservoir access and resource extraction. These wells facilitate the maximization of hydrocarbon recovery by allowing operators to tap into various zones within a reservoir while minimizing surface disruption. However, the complexities associated with ML well designs introduce unique challenges related to mechanical stability, which can jeopardize operational safety and economic viability. In deep wells, the prevailing conditions typically involve triaxial stress states, even in scenarios of symmetrical loading. The integrity and stability of these wells are critical and should not be overlooked [1]. Additionally, unconventional drilling techniques, such as ML wells, are pivotal in enhancing the efficiency and output of the parent well. ML wells are characterized by a horizontal or near-horizontal lateral well being drilled from the parent well, which can be further classified into two distinct levels:

1. New developments: Drilling a new well as an ML well (Figure 1)
2. Re-entries: Drilling new branches from the existing well [2], [3].

Advancements in drilling technologies have significantly increased production capacity per well and improved reservoir recovery factors. However, the intricate nature of ML well drilling introduces a higher likelihood of instability than traditional well designs. This necessitates a focused approach to wellbore stability, as it

* **Corresponding Author:** ghasemzadeh@kntu.ac.ir

remains one of the most critical challenges in the oil and gas sector [4], [5], [6], [7], [8], [9], [10], [11], [12]. Various engineering studies have addressed wellbore stability issues, but most have concentrated on single well configurations. The complex junctions and connections in ML wells present heightened risks that require thorough stability assessments. The two predominant types of instabilities—junction instability and bend instability—are vital contributors to the failure of ML wells [13], [14], [15].

Previous research on the stability of multilateral (ML) wells has predominantly focused on the drilling phase, employing both elastic [12], [15] and plastic models for mechanical analysis [16], [17] .However, as production progresses, the stress distribution and associated stability risks evolve due to fluid dynamics and depletion. Thus, evaluating the interplay between fluid flow and geomechanical factors is essential.

An appropriate failure criterion is essential for conducting a comprehensive mechanical analysis of well walls. This criterion should accurately assess the extent of potential failures in a manner that closely aligns with real-world observations.

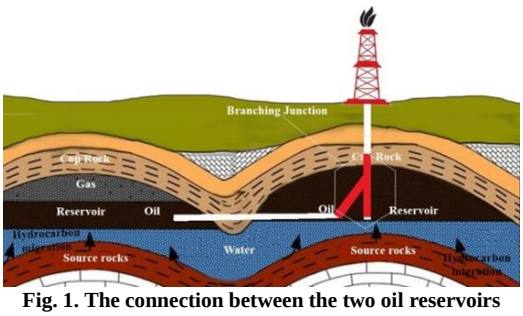

Fig. 1. The connection between the two oil reservoirs using ML wells

Most methodologies addressing wellbore stability primarily rely on linear elastic-brittle theory. According to this framework, borehole collapse is precipitated when elastic stresses exceed the material strength [18], [19], [20], [21], [22], [23], [24], [25]. Strength is typically characterized by a failure criterion, which, while advantageous for its simplicity and capability to handle anisotropic stress conditions, presents challenges in accurately modeling deformations. The failure criteria, rooted in the analysis of principal stresses, can be categorized into two main types:

a) Failure criteria excluding intermediate principal stress: This category includes models such as MC, Hoek-Brown, and Tresca, which do not consider the effects of the intermediate principal stress.

b) Failure criteria incorporating intermediate principal stress: This group encompasses criteria like Mogi-C, Drucker-Prager, and Lade, which explicitly factor in the influence of the intermediate principal stress on material failure.

Traditional failure criteria, such as the MC criterion, have been widely employed to assess wellbore stability. However, these criteria often overlook the significant role of intermediate principal stress (σ_2), which has been shown to impact mechanical failure mechanisms substantially [26], [27], [28], [29].

Recent studies have emphasized the importance of considering intermediate principal stress (σ_2) in stability analyses. Incorporating true triaxial stress states significantly improves the predictive capabilities of failure criteria in complex geological settings. On the other hand, integrating fluid dynamics into stability assessments is necessary, as fluid pressure variations can exacerbate mechanical instability in ML wells [30], [31], [32], [33], [34], [35], [36], [37], [38].

The Mohr-Coulomb failure criterion has gained prominence, particularly in the context of hard rocks [39]. However, its applicability to soft rocks remains questionable [40]. Characteristically, its failure envelope is linear rather than convex, which raises concerns given the mounting empirical data indicating otherwise. Existing criteria predominantly focus on the significant principal stresses, σ_1 and $\sigma3$, while neglecting the influence of $\sigma2$ for simplicity [41]. While this approach is often justified, in-situ stress measurements suggest that the stress states are typically anisotropic ($\sigma1\neq\sigma2\neq\sigma3$) [42], This observation supports the argument for employing polyaxial (three-dimensional or true-triaxial) failure criteria, particularly when $\sigma1>\sigma2>\sigma3$, as these may more accurately reflect the actual subsurface conditions compared to true-triaxial criteria where $\sigma1>\sigma2=\sigma3$ [43]. Moreover, recent studies[31], [32], [44], [45] highlight the significant role $\sigma2$ plays in rock failure, especially under conditions where the principal stresses are markedly disparate [46], [47]. Consequently, a variety of actual true-triaxial failure criteria have emerged over the past two decades [37], [48], [49], [50], [51], [52], [53], [54], [55], [56]. Noteworthy references in this domain include the works of Colmenares and Zoback, Benz and

Schwab, and Rukhaiyar and Samadhiya. [57], [58], [59]. However, it is worth noting that most true-triaxial criteria remain broadly applicable to rugged rocks, with limited relevancy for soft rock applications [60].

This study employs a three-dimensional finite element method (FEM) to analyze the stability of ML wells, utilizing both the Mogi-C and MC failure criteria for analysis due to their analogous formulations. By integrating the effects of intermediate principal stress, this research aims to provide a more accurate assessment of failure risks associated with ML well configurations.

2. Modelling open-hole ML wells

Due to the inherent asymmetry in the geometry of multi-layer (ML) wells, 3D numerical simulations are employed to assess deformation and failure mechanisms in these structures. Finite Element Method (FEM) analyses are utilized to investigate stress and deformation responses in well drilling scenarios, incorporating elastic, plastic, and elastoplastic material models [61], [62]. While 2D models can provide insights into the interactions between adjacent wells, they fail to accurately capture stress concentrations at convergence zones and account for stress rotations and flexural responses at junctions. Therefore, a comprehensive 3D hydro-mechanical FEM approach is implemented, integrating elastic deformations with Darcy flow to compute stress-strain distributions and pore pressures across the entire 3D domain. This methodology accounts for in situ stresses (σx, σy, σz), reservoir pressure (Pr), and well pressure (Pw), thereby offering a holistic view of the well's performance under various loading conditions.

2.1. Failure Criterion

2.1.1. Mohr-Coloumb failure criterion

The classical Mohr-Coulomb (MC) failure criterion is a linear model for shear failure, characterized by two fundamental parameters: cohesion (C) and friction angle (ϕ). In the context of normal stress (σ) and shear stress (τ), the MC criterion can be mathematically expressed as:

$$\tau - C - \sigma_n . \tan\phi = 0 \qquad (1)$$

In principal stress space (σ_1, σ_3), the classical Mohr-Coulomb (MC) failure criterion can be reformulated as:

$$\sigma_1 - \frac{1+\sin\phi}{1-\sin\phi}\sigma_3 - \frac{2C\cos\phi}{1-\sin\phi} = 0 \qquad (2)$$

In line with Equation 2, when the maximum stress (σ_{max}) is zero, the tensile strength (σ_T) can be represented by Equation 3. Conversely, if the minimum stress (σ_{min}) is zero, the compressive strength (σ_c) is defined by Equation 4.

$$\sigma_3 = \frac{-2C\cos\phi}{1+\sin\phi} = \sigma_T \qquad (3)$$

$$\sigma_1 = \frac{2C\cos\phi}{1-\sin\phi} = \sigma_c \qquad (4)$$

According to Equations 3 and 4, the ratio between σc and σT can be expressed by the following Equation:

$$\frac{\sigma_c}{\sigma_T} = \frac{1+\sin\phi}{1-\sin\phi} = q \qquad (5)$$

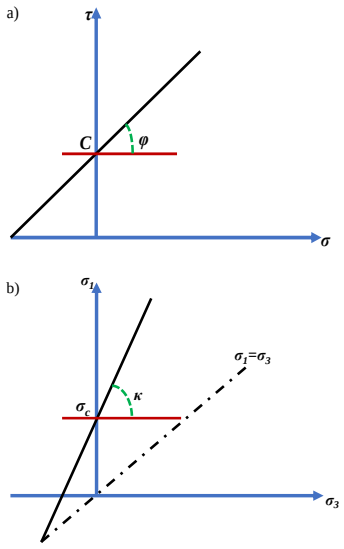

Fig 2: Classical MC failure criterion in the normal stress-shear stress space (a) and the principal stress field (b)

The ratio of compressional stress (σ_c) to tensile stress (σ_T) is a critical parameter in understanding the mechanical behavior of materials under various loading conditions. Compressional stress is induced when forces compress a material, while tensile stress arises from forces that extend or pull it apart. Analyzing this ratio yields essential insights into a material's mechanical properties.

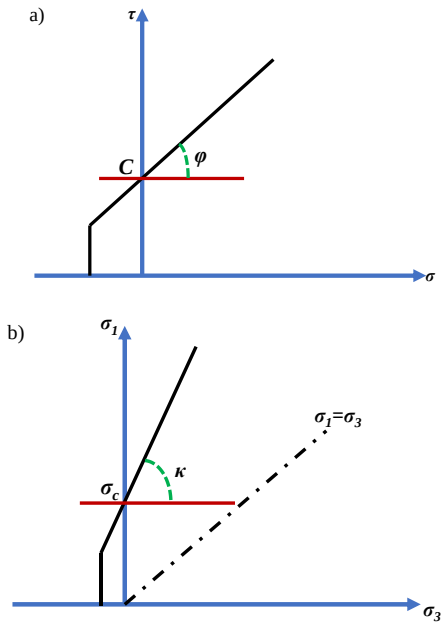

Fig 3: MC failure criterion with stress removal in the normal stress-shear stress space (a) and the principal stress field (b)

Materials exhibiting a high compressional-to-tensile stress ratio typically demonstrate excellent resistance to compressive forces and are prone to brittle failure. Conversely, materials with a low ratio tend to undergo significant plastic deformation under compressive loads.

This understanding is crucial for engineers and designers in material selection tailored to specific applications, as it directly impacts the strength and stability of structures. For instance, materials with a balanced compressional-to-tensile stress ratio are often preferred to enhance safety and durability, ensuring structures can effectively withstand both tensile and compressive forces.

Assuming realistic friction angle values, the calculated resistance ratio (q), as per Equation 5, tends to be lower than the values derived from empirical measurements. The applicability of the classic Mohr-Coulomb (MC) criterion in rock mechanics, illustrated in Figure 3, is frequently constrained by the stress limit criterion $\sigma_3 = \sigma_T$, which is directly obtained from observational data.

2.1.2. Mogi-C Failure Criterion

Principal stresses play a significant role in determining the Unconfined Compressive Strength (UCS) of rocks [63]. Mogi (1971) introduced the concept of Fracture Criterion (FC) as outlined in Equation 6, emphasizing the influence of the second principal stress (σ2) on rock fracturing mechanisms [45], [57].

$$A\left(\frac{\sigma_1-\sigma_3}{2}\right)^n-\tau_{OCT}=0 \quad (6)$$

where:

$$\tau_{OCT}=\frac{1}{3}\sqrt{(\sigma_1-\sigma_2)^2+(\sigma_2-\sigma_3)^2+(\sigma_3-\sigma_1)^2} \quad (7)$$

In Equation 6, A and n are material parameters obtained by curve fitting. However, this criterion was debatable because the material parameters could not be related to the MC failure parameters. Al-Ajmi & Zimmerman (2005) introduced a linear criterion called Mogi-C, as described in Equation 8 [45], [56]:

$$a+b\left(\frac{\sigma_1+\sigma_3}{2}\right)-\tau_{OCT}=0 \quad (8)$$

In Equation 8, the parameters a and b are expressed as functions of the MC parameters, specifically C and ϕ, as delineated in Equations 9 and 10.

$$a=\frac{2\sqrt{2}}{3}C\cos\phi \quad (9)$$

$$b=\frac{2\sqrt{2}}{3}\sin\phi \quad (10)$$

We present $\sigma_{m,2}$ as the average of the maximum and minimum principal stresses. The formulation in equation 8 can be succinctly summarized as follows:

$$a+b\sigma_{m,2}-\tau_{OCT}=0 \quad (11)$$

In the Mogi-C criterion, when the second principal stress (σ_2) equals either the maximum principal stress ($\sigma_1=\sigma_2$) or the minimum principal stress ($\sigma_2=\sigma_3$), the criterion simplifies to the linear equation characteristic of the MC failure criteria.

By applying Terzaghi's effective stress principle ($\sigma' = \sigma - p$), Equation 11 can be reformulated as follows:

$$a+b(\sigma_{m,2}-p)-\tau_{OCT}=0 \quad (12)$$

Finally, the failure function can be written as:

$$\text{Fail}=\frac{\tau_{OCT}}{a}-\frac{b}{a}(\sigma_{m,2}-p) \quad (13)$$

For a given stress situation, if Fail ≥ 1, it denotes failure of the rock, and if Fail < 1, it predicts the stability of the rock.

2.2.Geometry and material properties

In this numerical simulation, we model a 22 cm diameter ML well (The usual diameter of oil wells at deep depths) situated within a 4-meter cubic block surrounding the red ML depicted in Figure

1. To streamline the computational process, we employed a symmetry plane, as illustrated in Figure 4-a, effectively bisecting the model. The finite element mesh for the computational domain is provided in Figure 4-b. Details regarding the rock properties and reservoir characteristics are delineated in Tables 1 and 2.

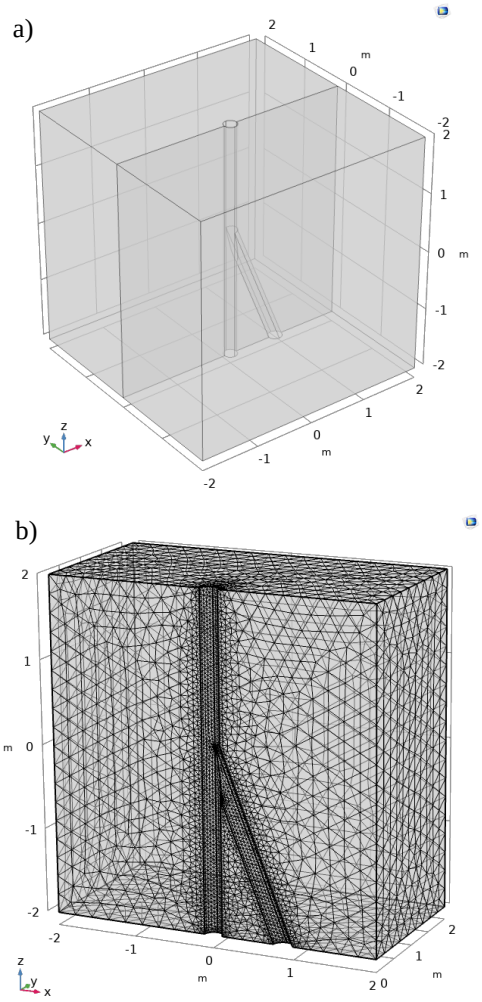

Fig 4: a) Area around the branch joints for numerical simulation, b) The complete meshing of the model

Table 1. Mechanical Rock Properties

VARIABLE	*DESCRIPTION*	*Value*	*Unit*
ρ_s	Solids density	2560	kg/m^3
E	Young's modulus	11	*GPa*
v	Poisson's ratio	0.31	-
C	Cohesion	4	*MPa*
ϕ	Friction angle	30 and 45	*deg*
n	Porosity	0.15	-

Table 2. Fluid Properties Parameters

VARIABLE	DESCRIPTION	Value	Unit
ρ_f	Fluid density	830	kg/m^3
μ	Fluid dynamic viscosity	2.439e-3	*Pa.s*
k	Permeability	8.5	*md*
p_r	Por-pressure	31	*MPa*
C_f	Compressibility of fluid	1.4504e-9	*1/Pa*
α	Biot-Willis coefficient	0.75	-
p_w	Mud pressure	[0-10-15-20-25-30-35-40]	*MPa*

2.3. Boundary conditions and model assumptions

One of the essential parts of achieving reliable results in numerical methods is considering the correct boundary conditions. In this study, the boundary conditions are such that the only fluid outlet is through the well, so the boundaries perpendicular to the axis of the well are considered without fluid flow. The wellhead can deform in terms of deformation, but the side walls cannot deform.

2.3.1. Physical formulation of fluid flow

According to the porous medium's governing equations, fluid flow in the porous medium can be expressed using a combination of the continuity equation and the Darcy equation, as shown in Equation 14.

$$\nabla.\left(-\frac{k}{\mu}\nabla p_f\right)=0 \qquad (14)$$

In Equation 14, k is the intrinsic permeability, μ is the dynamic viscosity, and P_f is the pore fluid pressure. The pore pressure within the reservoir will change when production begins. Because when the pumping starts, a pressure drop occurs around the walls, and the fluid sucks into this part, which will cause a pore-pressure decline in different parts. Since the well is the only outlet for fluid, networks do not pass through well junctions or the well [64, 65]. In summary:

$$p = p_{reservoir} \qquad \partial\Omega \text{ Reservoir} \qquad (15)$$

$$n.\left(-\frac{\kappa}{\mu}\nabla p\right)=0 \quad \partial\Omega \text{ Symmetry face}$$
$$n.\left(-\frac{\kappa}{\mu}\nabla p\right)=0 \quad \partial\Omega \text{ Connecting segments} \qquad (16)$$

$$p = p_w \qquad \partial\Omega \text{ Well} \qquad (17)$$

where n is the normal vector to the boundary, and $\partial\Omega$ represents the range.

2.3.2. Physical formulation of solid deformation

Pressure changes cause solid deformation because the Cauchy stress tensor is related to the pore pressure as follows [65, 66]:

$$\sigma = C\,\varepsilon - \alpha_B p_f I \tag{18}$$

where C is the elasticity matrix that depends on Young's modulus (E) and Poisson's ratio (v), ε is the strain tensor, and α is the Biot coefficient. Equation 19 is the linear momentum balance equation of the whole system, where F is the body force vector.

$$-\nabla.\sigma = F$$

$$\sigma = \begin{bmatrix} \sigma_x & \tau_{xy} & \tau_{xz} \\ \tau_{yx} & \sigma_y & \tau_{yz} \\ \tau_{zx} & \tau_{zy} & \sigma_z \end{bmatrix} \tag{19}$$

The stress-strain equation for linear materials relates the stress tensor σ to the strain tensor ε through the elasticity matrix C, which is a function of E, and v for isotropic materials.

In the linear geometric model of this research, the strain tensor components depend on the displacement vector u, which includes directional components u, v, and w:

$$\begin{aligned} \varepsilon_x &= \frac{\partial u}{\partial x} & \varepsilon_{xy} &= \frac{1}{2}\left(\frac{\partial u}{\partial y} + \frac{\partial v}{\partial x}\right) \\ \varepsilon_y &= \frac{\partial v}{\partial y} & \varepsilon_{yz} &= \frac{1}{2}\left(\frac{\partial v}{\partial z} + \frac{\partial w}{\partial y}\right) \\ \varepsilon_z &= \frac{\partial w}{\partial z} & \varepsilon_{xz} &= \frac{1}{2}\left(\frac{\partial u}{\partial z} + \frac{\partial w}{\partial x}\right) \end{aligned} \tag{20}$$

Also, in Figure 5, a summary of the boundary conditions is presented for the model.

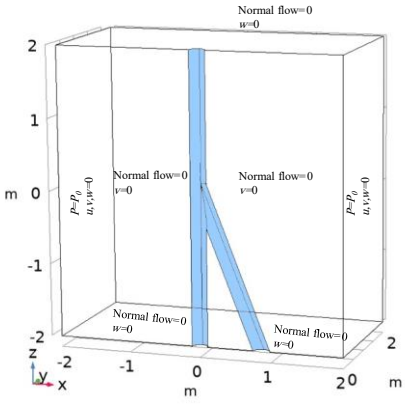

Fig 5: GEometry and the boundary conditions

3. Simulation results

3.1. Solid displacement and deformation

Figure 6 provides a critical visualization of the displacement behavior in open-hole ML wells as a function of varying intra-well pressures (mud pressures). This graph is essential for understanding how pressure changes affect the structural integrity of the wellbore and surrounding geological formations.

The graph illustrates a clear trend where total displacement decreases as intra-well pressure increases. This indicates that higher pressures can initially stabilize the wellbore by reducing the amount of movement or deformation in the surrounding rock. On the other hand, the isosurface representation allows for a three-dimensional view of how displacement varies spatially around the wellbore, providing insights into which areas are most affected by pressure changes.

A significant observation from the graph is the critical threshold at 30 MPa. As pressures exceed this level, the graph indicates the formation of concentrated stress zones around the wellbore. The graph highlights these zones, showing areas where the displacement is reduced and where stress concentrations could lead to potential failure. Identifying this threshold is crucial for drilling operations, as it suggests that increasing pressure can help maintain stability, but it poses risks if not carefully managed.

Moreover, The graph emphasizes the delicate balance between maintaining sufficient pressure to prevent shear failure and avoiding excessive pressure that could induce tensile failure or hydraulic fracturing. This balance is visually represented by the displacement patterns observed in the isosurface. The areas of concentrated stress around the wellbore, particularly when pressures exceed 30 MPa, indicate potential failure zones. This insight is vital for engineers and geoscientists as they design and monitor drilling operations.

3.2. Fluid distribution and pressure

The Pressure Isosurface in the graph of Figure 7 provides a detailed visualization of the pressure distribution around the wellbore under various pressure conditions ($Pw \leq 30$ MPa). This graph is crucial for understanding fluid flow dynamics and pressure behavior in open-hole ML wells, particularly underbalanced drilling scenarios.

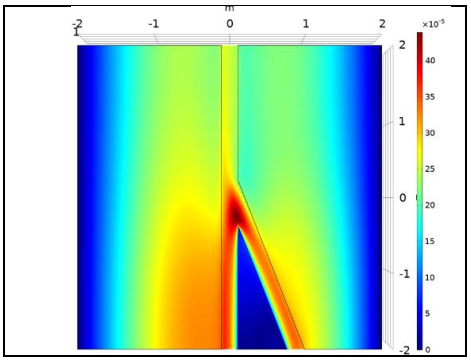

Pw=0MPa

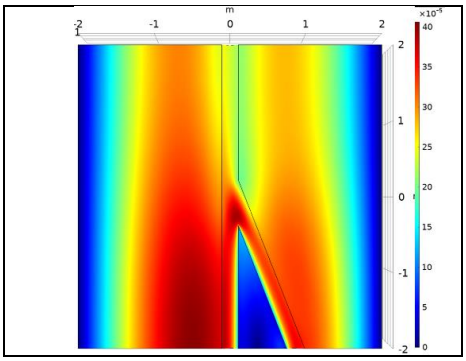

Pw=10MPa

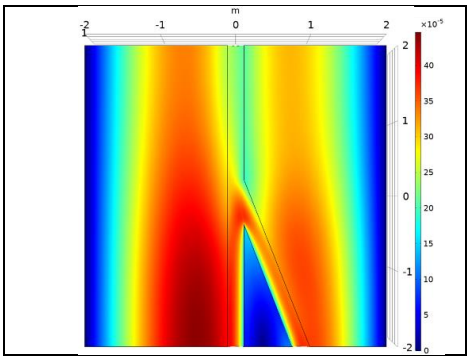

Pw=15MPa

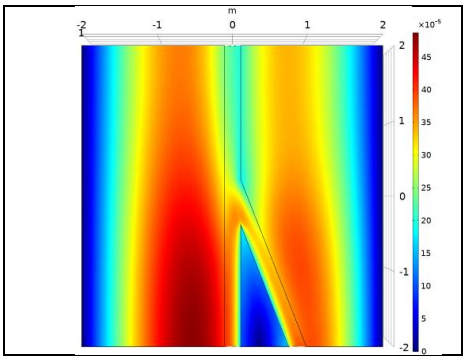

P=20MPa

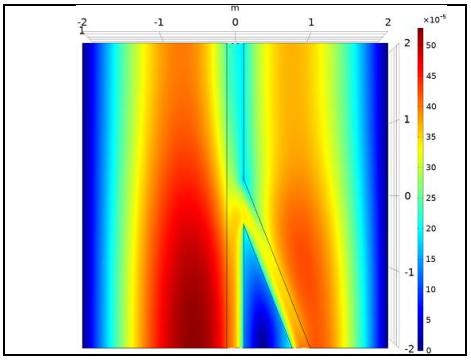

Pw=25MPa

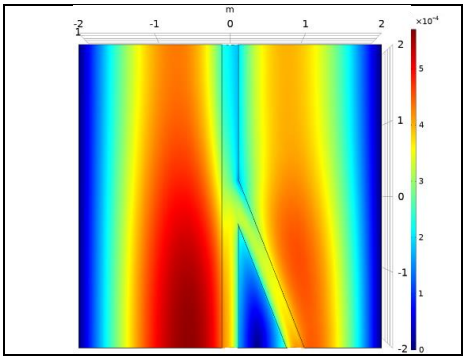

Pw=30MPa

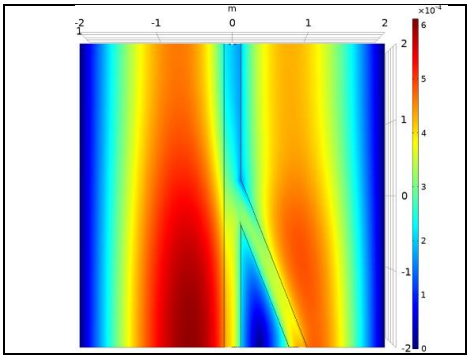

Pw=35MPa

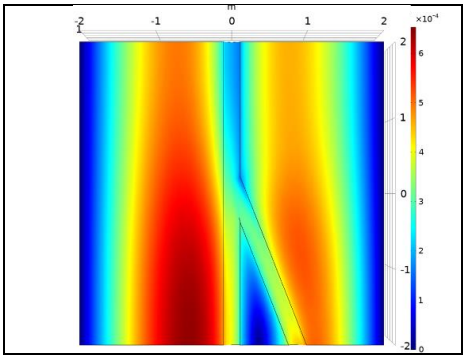

Pw=40MPa

Fig 6: Total displacement isosurface around the well (m)

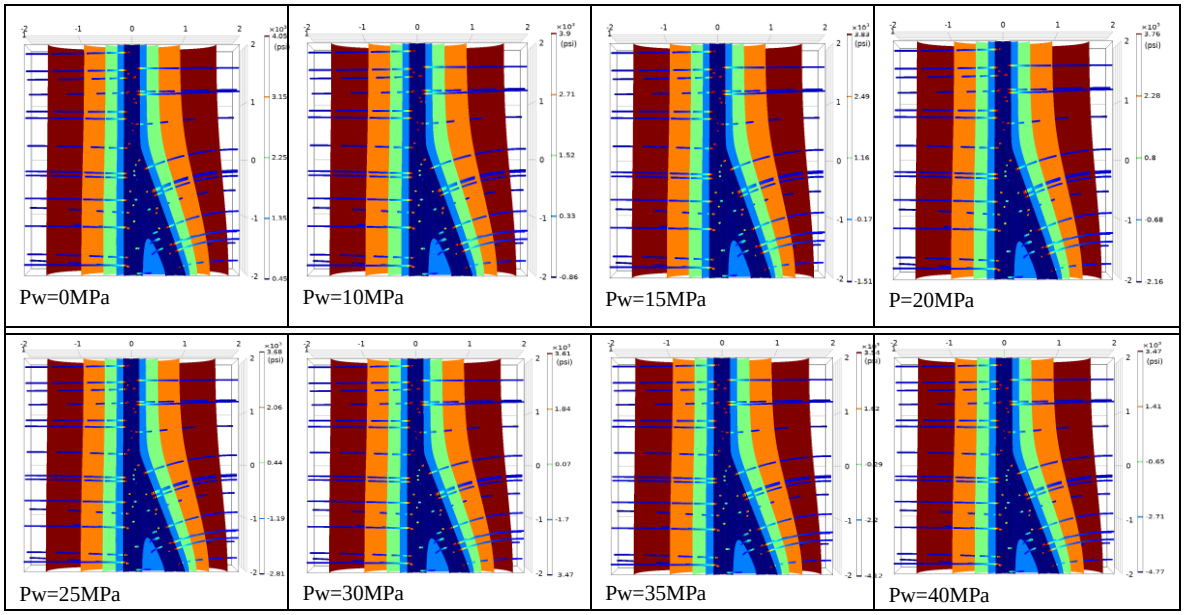

Fig 7: Pressure isosurface changes and streamlines around the well

The graph of Figure 7 illustrates that the borehole pressure is significantly lower than the pore pressure, characterizing an underbalanced drilling scenario. This condition is visually represented through color gradients and isosurfaces, indicating that the pressure within the well consistently lags behind the surrounding pore pressure. The pressure differential is critical as it facilitates the ingress of pore fluid into the wellbore. The streamlines visually depict this influx, indicating the fluids' direction and flow toward the wellbore.

The pressure drop near the borehole promotes fluid migration into the well. This factor is particularly important in drilling operations as it can enhance the efficiency of fluid extraction and reservoir management. The streamlines in the graph effectively illustrate how fluids are drawn into the wellbore, thereby highlighting the advantages of underbalanced drilling in specific contexts. However, the graph is also a cautionary note, as excessive fluid migration may lead to instability if not managed with care. The visual representation of fluid movement underscores the need for precise control over pressure conditions to prevent potential wellbore collapse or other mechanical failures.

Furthermore, the graph indicates that substantial pressure gradients surrounding the well can result in notable displacement phenomena near the wellbore wall and at the branch interface. This information is crucial for understanding how pressure variations impact the well's structural integrity. The visual data suggest that while maintaining lower pressures can facilitate fluid influx, it simultaneously necessitates vigilant monitoring to prevent the emergence of conditions that could compromise stability or lead to failure.

The graph permits a comparative analysis of varying pressure conditions (Pw = 0 MPa to Pw = 30 MPa). As pressure increases, the distribution patterns evolve, which can be correlated with the stability of the wellbore. Visualizing these changes provides insights into how different pressure levels can influence the mechanical behavior of the well and the efficacy of fluid extraction strategies. The graph emphasizes the critical importance of managing pressure differentials during drilling operations. Operators must carefully balance the benefits of underbalanced drilling with the risks associated with excessive fluid influx and potential instability. Moreover, the pressure isosurface and streamlines serve as diagnostic tools for engineers, aiding in the visualization and prediction of fluid behavior within the wellbore. This capability can guide real-time decision-making during drilling operations and enhance safety protocols.

The findings derived from this graph underscore the necessity of incorporating advanced modeling techniques that account for fluid dynamics and pressure distributions in well design. A comprehensive understanding of these dynamics is essential for optimizing drilling operations and ensuring the long-term stability of multilateral wells.

3.3. Effects of Intermediate Principal Stress

Graphs depicted in Figure 8 offer a comparative analysis of failure predictions for ML wells utilizing two distinct failure criteria: the Mogi-C criterion, which accounts for the influence of intermediate principal stress (σ_2), and the conventional MC criterion, which does not include this parameter. This analysis is critical for comprehending how these criteria affect the evaluation of well stability and associated failure risks.

.

This graph delineates five distinct boundaries (A, B, C, D, and E) along the surface of the well wall, identifying four zones predisposed to failure. Each zone exhibits varying degrees of susceptibility, with Zone 1 demonstrating the highest severity and frequency of failure incidents. The Mogi-C criterion indicates a lower number of predicted failure points compared to the MC criterion, particularly in areas where the MC criterion suggests potential failure. This disparity underscores the conservative nature of the MC criterion, which may lead to excessive caution in well-designed and operational practice

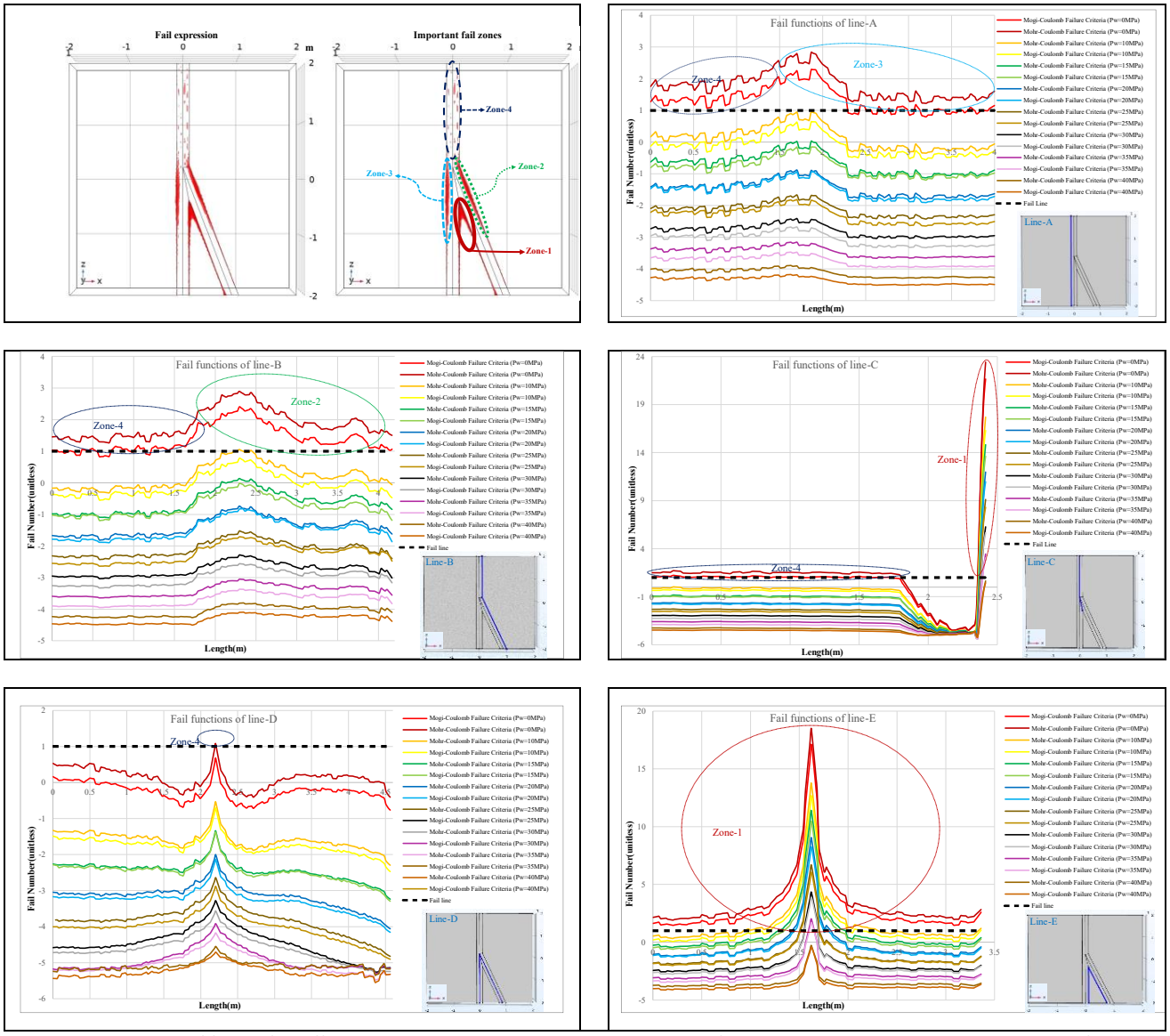

Fig 8: Investigation of failure for different borehole pressures using Mogi-C and MC failure criteria (all red parts have undergone failure)

conversely, incorporating σ_2 in the Mogi-C criterion substantially modifies the failure predictions. The graph illustrates that the Mogi-C criterion offers a more accurate evaluation of failure risks, especially at the junctions of the branches, where mechanical failures are more likely to arise. By excluding σ_2, the MC criterion frequently forecasts failure in locations where the Mogi-C criterion does not, suggesting that the MC approach may inadequately account for the complexities of stress interactions in ML wells.

Identifying failure-prone zones is essential for determining where targeted interventions may be required during drilling operations. The graph indicates that Zone 1 is particularly vulnerable, implying that focused engineering solutions should be implemented in this area to enhance stability. As illustrated in the graph, the persistence of failures at the branch junctions across all pressure ranges emphasizes the need for concentrated attention during the design and drilling phases of ML wells.

The insights derived from this graph advocate for a paradigm shift in wellbore stability analysis. By integrating intermediate principal stress into stability assessments, operators can better understand failure mechanisms, leading to improved safety protocols and optimized drilling operations. Furthermore, the graph serves as a visual representation of the significant role of advanced modeling techniques in predicting well stability, reinforcing the imperative to incorporate these methodologies into standard practices within the oil and gas industry.

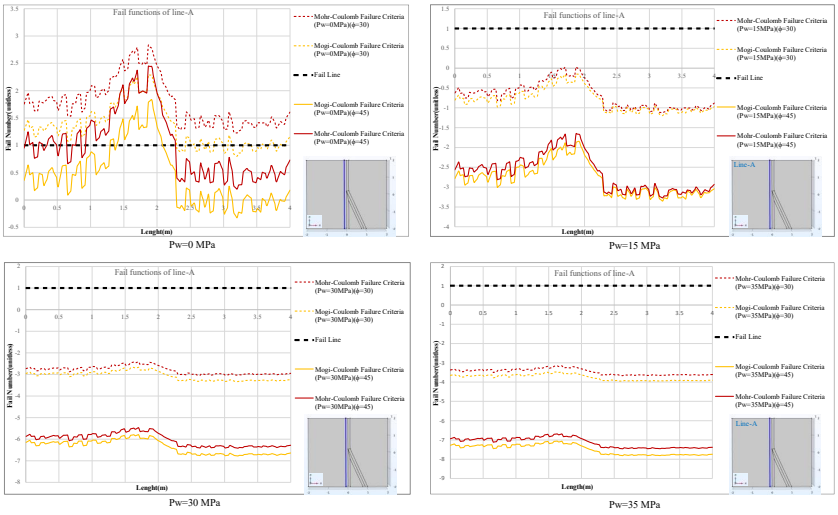

Fig 9.1: Prediction of sensitive range in ML wells using Mogi-C criterion and MC criterion (Line A)

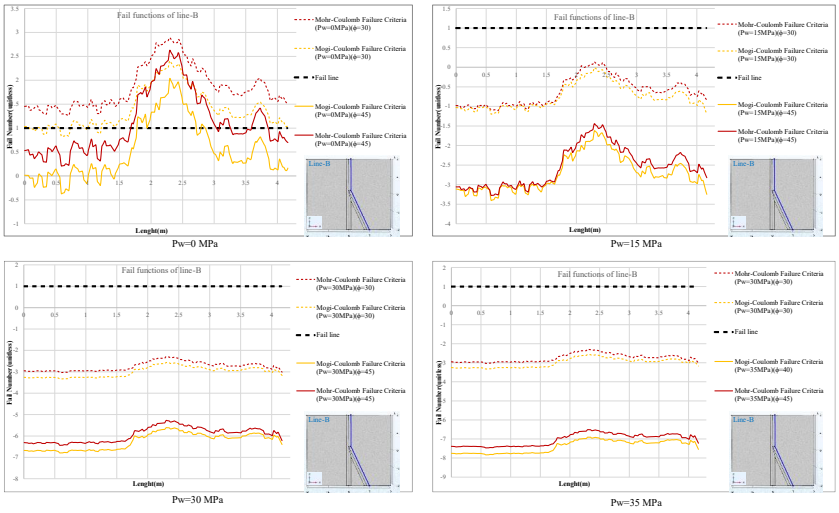

Fig 9.2: Prediction of sensitive range in ML wells using Mogi-C criterion and MC criterion (Line B)

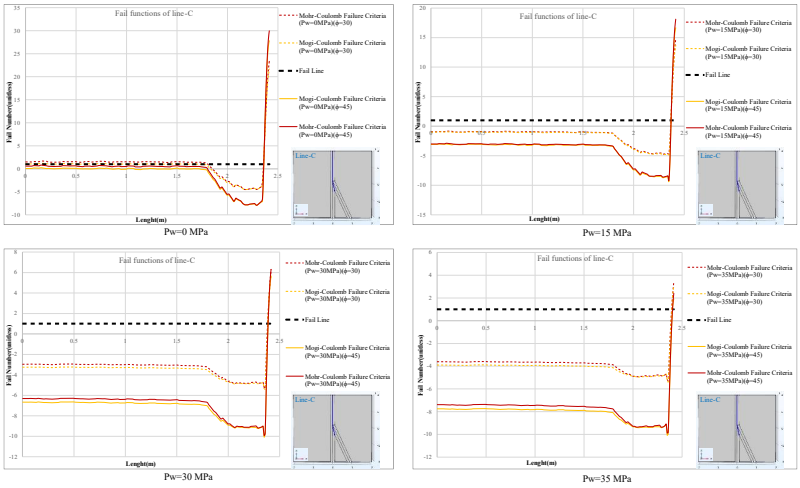

Fig 9.3: Prediction of sensitive range in ML wells using Mogi-C criterion and MC criterion(Line C)

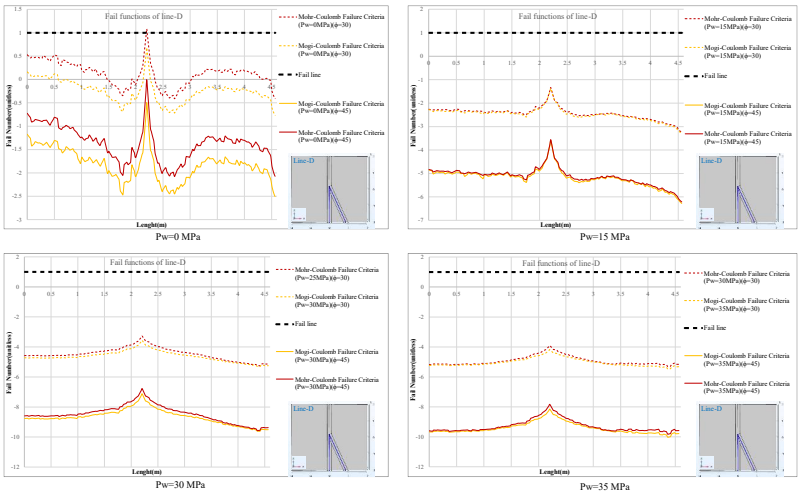

Fig 9.4: Prediction of sensitive range in ML wells using Mogi-C criterion and MC criterion (Line D)

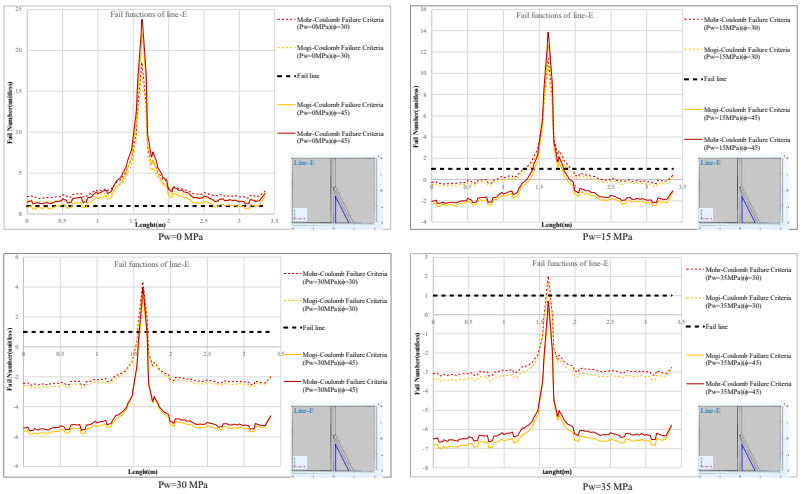

Fig 9.5: Prediction of sensitive range in ML wells using Mogi-C criterion and MC criterion (Line E)

Lines A, B, C, D, and E of the graph in Figure 9 represent diverse failure functions derived from the Mogi-C and Mohr-Coulomb failure criteria under varying borehole pressures (Pw). Each line provides critical insights into the influence of pressure on the probability of failure in the surrounding geological material, highlighting significant thresholds and zones of potential failure.

Line A of Figure 9.1 demonstrates distinct failure patterns under various pressures, indicating that certain pressure levels markedly increase the incidence of failures. The failure functions associated with the Mogi-C and Mohr-Coulomb criteria illustrate the material's behavior under low to moderate pressures. This analysis identifies critical thresholds, particularly at pressures around 20 MPa and above, emphasizing the necessity for monitoring and potential reinforcement in these areas. Specific regions, such as Zone 1 and Zone 4, are identified as vulnerable, suggesting the need for proactive measures to avert structural failure.

Line B of Figure 9.2 similarly indicates that an increase in pressure correlates with changes in failure numbers, reinforcing the relationship between pressure and the likelihood of failure. The failure functions reveal a significant escalation in failure numbers at elevated pressure levels, particularly around 25 MPa, necessitating careful management to mitigate risks. Highlighted failure zones, including Zone 2 and Zone 4, offer insight into where intervention may be warranted, aligning with observations made in Line A.

Line C of Figure 9.3 further elucidates the impact of pressure on the likelihood of failure, suggesting that certain pressure levels are more critical than others, precisely at 30 MPa and above. The patterns indicate that specific pressures increase in failure numbers, thus aiding in predicting potential failure points, especially within Zones 1 and 4. This line also identifies zones that require proactive measures to enhance safety and stability, consistent with the findings from Lines A and B.

Line D of Figure 9.4 exhibits the observed trend, illustrating how varying pressures influence failure functions, with data indicating notable variations in structural response. The failure functions consistently show an increase in failure numbers alongside pressure increases. This analysis underscores the necessity for continuous monitoring of borehole pressures, as the likelihood of failure exhibits significant variability with pressure fluctuations, particularly at pressures exceeding 35 MPa. Like the previous lines, Line D emphasizes critical zones, particularly Zone 4, that may necessitate fortification or heightened monitoring to prevent failure.

Line E of Figure 9.5 presents failure functions in alignment with the trends identified in earlier lines, indicating a continuous pattern where increased pressure correlates with heightened failure numbers. The functions demonstrate a consistent upward trend in failure likelihood with increasing pressure. The findings convey the importance of meticulously managing borehole pressures to sustain structural integrity and deter failures, particularly at approximately 40 MPa. Consistent with the findings from other lines, Line E recognizes critical failure zones, emphasizing the importance of monitoring and potential interventions, especially in Zones 1 and 4.

Collectively, all five lines illustrate a consistent trend wherein increased borehole pressure is associated with a higher likelihood of failure, thereby establishing a clear relationship between pressure and failure probability. Each line delineates specific pressure levels critical for safe operations, highlighting the importance of monitoring these thresholds to prevent structural failures. The vital pressures exhibit a general increase from Line A to Line E, reflecting a more pronounced sensitivity to pressure changes. Furthermore, all lines underscore the importance of identifying zones where materials are particularly prone to failure, suggesting that proactive measures are essential across all scenarios. Zones 1, 2, 3, and 4 are consistently highlighted as areas of concern.

Failures, particularly at approximately 40 MPa. Consistent with the findings from other lines, Line E recognizes critical failure zones, emphasizing the importance of monitoring and potential interventions, especially in Zones 1 and 4.

4. Conclusions

This study evaluates the stability of open-hole multilateral wells, focusing on the impact of intermediate principal stress. By assessing the predictive capabilities of the Mogi-C criterion in comparison to the Mohr-Coulomb criterion, the analysis demonstrates that the incorporation of intermediate principal stress via the Mogi-C criterion substantially enhances stability predictions across various pressure conditions. Specifically, at pressures exceeding 30 MPa, the Mogi-C criterion exhibits a significant reduction of approximately 30% in predicted failure points when contrasted with the Mohr-Coulomb

criterion. At a benchmark pressure of 35 MPa, the anticipated incidence of failures declines from approximately 15%, as predicted by the Mohr-Coulomb criterion, to merely about 5% with the Mogi-C criterion. These results underscore the crucial role of intermediate principal stress in accurately modeling multilateral well stability. The considerable improvements observed through the application of the Mogi-C criterion suggest that its implementation may facilitate safer and more efficient drilling practices. By integrating intermediate principal stress into stability assessments, a robust framework for predicting well integrity is established, thereby enhancing operational decision-making and risk management in multilateral drilling initiatives.

4. References

[1] A. Singh, K. S. Rao, and R. Ayothiraman, "An analytical solution to wellbore stability using Mogi-Coulomb failure criterion," *J. Rock Mech. Geotech. Eng.*, vol. 11, no. 6, 2019, doi: 10.1016/j.jrmge.2019.03.004.

[2] P. A. Charlez and P. Breant, "Multiple role of unconventional drilling technologies. From well design to well productivity," *SPE - Eur. Form. Damage Control Conf. Proc.*, 1999, doi: 10.2523/56405-ms.

[3] I. Tantawi, R. Taylor, and R. Russell, "The successful redevelopment of existing wells using multilateral drilling techniques," in *Society of Petroleum Engineers - Abu Dhabi International Petroleum Exhibition and Conference 1998, ADIPEC 1998*, 1998. doi: 10.2118/49477-ms.

[4] M. Salarian, A. Mirzaghorbanali, H. Ghasemzadeh, and S. Sadeghian, "Well Bore Stability Using a New Dynamic Model," *Pet. Sci. Technol.*, vol. 30, no. 19, pp. 2066–2075, Jul. 2012, doi: 10.1080/10916466.2010.512891.

[5] A. Mirzaghorbanali, N. Fathianpour, H. Ghasemzadeh, and M. Salarian, "A New Approach in Casing Collapse Design Using the Geomechanical Model and Heaviest Drilling Fluid," *Pet. Sci. Technol.*, vol. 29, no. 18, pp. 1948–1962, Jul. 2011, doi: 10.1080/10916461003663024.

[6] M. Frydman and S. A. B. da Fontoura, "Applications of a coupled chemical-hydro-mechanical model to wellbore stability in shales," 2000.

[7] E. Kaarstad and B. Aadnoy, "Optimization of Borehole Stability Using 3D Stress Optimization," in *Proceedings of SPE Annual Technical Conference and Exhibition*, Society of Petroleum Engineers, Oct. 2005. doi: 10.2523/97149-MS.

[8] C. D. Hawkes, "Assessing the mechanical stability of horizontal boreholes in coal," *Can. Geotech. J.*, vol. 44, no. 7, pp. 797–813, Jul. 2007, doi: 10.1139/t07-021.

[9] B. Pašić, N. Gaurina-Medimurec, and D. Matanović, "Wellbore instability: Causes and consequences," *Rud. Geol. Naft. Zb.*, vol. 19, 2007.

[10] K. Ahmed, K. Khan, and M. A. Mohamad-Hussein, "Prediction of Wellbore Stability Using 3D Finite Element Model in a Shallow Unconsolidated Heavy-Oil Sand in a Kuwait Field," in *All Days*, SPE, Mar. 2009. doi: 10.2118/120219-MS.

[11] Y. Zhang, A. Long, Y. Zhao, A. Zang, and C. Wang, "Mutual impact of true triaxial stress, borehole orientation and bedding inclination on laboratory hydraulic fracturing of Lushan shale," *J. Rock Mech. Geotech. Eng.*, vol. 15, no. 12, 2023, doi: 10.1016/j.jrmge.2023.02.015.

[12] B. S. Aadnoy and C. Edland, "Borehole stability of multilateral junctions," *J. Pet. Sci. Eng.*, vol. 30, no. 3–4, 2001, doi: 10.1016/S0920-4105(01)00137-1.

[13] R. Brister, "Screening Variables for Multilateral Technology," in *Proceedings of the International Oil and Gas Conference and Exhibition in China, IOGCEC*, 2000. doi: 10.2118/64698-ms.

[14] H. Xu, J. Cao, L. Dong, and C. Yan, "Study on Wellbore Stability of Multilateral Wells under Seepage-Stress Coupling Condition Based on Finite Element Simulation," 2023. doi: 10.3390/pr11061651.

[15] H. Bargui and Y. Abousleiman, "2D and 3D elastic and poroelastic stress analyses for multilateral wellbore junctions," in *4th North American Rock Mechanics Symposium, NARMS 2000*, 2000.

[16] A. L. Manríquez, A. L. Podio, and K. Sepehrnoori, "Modeling of stability of junctions in multilateral wells using finite element," in *42nd U.S. Rock Mechanics - 2nd U.S.-Canada Rock Mechanics Symposium*, 2008.

[17] B. Plischke, N. Kågeson-Loe, O. Havmøller, H. F. Christensen, and M. G. Stage, "Analysis of MLW open hole junction stability," in *Gulf Rocks 2004 - 6th North America Rock Mechanics Symposium, NARMS 2004*, 2004.

[18] E. Detournay and A. H. D. Cheng, "Poroelastic response of a borehole in a non-hydrostatic stress field," *Int. J. Rock Mech. Min. Sci. Geomech. Abstr.*, vol. 25, no. 3, pp. 171–182, Jun. 1988, doi: 10.1016/0148-9062(88)92299-1.

[19] L. Cui, A. H. D. Cheng, and Y. Abousleiman, "Poroelastic solution for an inclined borehole," *J. Appl. Mech. Trans. ASME*, vol. 64, no. 1, 1997, doi: 10.1115/1.2787291.

[20] Y. Abousleiman and L. Cui, "Poroelastic solutions in transversely isotropic media for wellbore and cylinder," *Int. J. Solids Struct.*, vol. 35, no. 34–35, pp. 4905–4929, Dec. 1998, doi: 10.1016/S0020-7683(98)00101-2.

[21] A. M. Al-Ajmi and R. W. Zimmerman, "Stability analysis of vertical boreholes using the Mogi–Coulomb failure criterion," *Int. J. Rock Mech. Min. Sci.*, vol. 43, no. 8, pp. 1200–1211, Dec. 2006, doi: 10.1016/J.IJRMMS.2006.04.001.

[22] N. Tang-Tat, "Particle shape effect on macro- and micro-behaviors of monodisperse ellipsoids," *Int. J. Numer. Anal. Methods Geomech.*, vol. 33, no. 4, 2009, doi: 10.1002/nag.732.

[23] M. R. Zare-Reisabadi, A. Kaffash, and S. R. Shadizadeh, "Determination of optimal well trajectory during drilling and production based on borehole stability," *Int. J. Rock Mech. Min. Sci.*, vol. 56, pp. 77–87, Dec. 2012, doi: 10.1016/J.IJRMMS.2012.07.018.

[24] W. Zhang, J. Gao, K. Lan, X. Liu, G. Feng, and Q.

Ma, “Analysis of borehole collapse and fracture initiation positions and drilling trajectory optimization,” *J. Pet. Sci. Eng.*, vol. 129, pp. 29–39, May 2015, doi: 10.1016/J.PETROL.2014.08.021.

[25] B. Das and R. Chatterjee, “Wellbore stability analysis and prediction of minimum mud weight for few wells in Krishna-Godavari Basin, India,” *Int. J. Rock Mech. Min. Sci.*, vol. 93, pp. 30–37, Mar. 2017, doi: 10.1016/J.IJRMMS.2016.12.018.

[26] E. Detournay, “Elastoplastic model of a deep tunnel for a rock with variable dilatancy,” *Rock Mech. Rock Eng.*, vol. 19, no. 2, 1986, doi: 10.1007/BF01042527.

[27] M. E. D. Fama, “Numerical Modeling of Yield Zones in Weak Rock,” *Compr. rock Eng. Vol. 2*, pp. 49–75, Jan. 1993, doi: 10.1016/B978-0-08-040615-2.50009-5.

[28] X.-D. Pan and E. T. Brown, “Influence of Axial Stress and Dilatancy on Rock Tunnel Stability,” *J. Geotech. Eng.*, vol. 122, no. 2, 1996, doi: 10.1061/(asce)0733-9410(1996)122:2(139).

[29] C. Carranza-Torres, “Dimensionless graphical representation of the exact elastoplastic solution of a circular tunnel in a Mohr-Coulomb material subject to uniform far-field stresses,” *Rock Mech. Rock Eng.*, vol. 36, no. 3, 2003, doi: 10.1007/s00603-002-0048-7.

[30] K. Mogi, “Effect of the triaxial stress system on the failure of dolomite and limestone,” *Tectonophysics*, vol. 11, no. 2, pp. 111–127, Feb. 1971, doi: 10.1016/0040-1951(71)90059-X.

[31] C. Chang and B. Haimson, “True triaxial strength and deformability of the German Continental Deep Drilling Program (KTB) deep hole amphibolite,” *J. Geophys. Res. Solid Earth*, vol. 105, no. B8, 2000, doi: 10.1029/2000jb900184.

[32] B. Haimson and C. Chang, “A new true triaxial cell for testing mechanical properties of rock, and its use to determine rock strength and deformability of Westerly granite,” *Int. J. Rock Mech. Min. Sci.*, vol. 37, no. 1–2, pp. 285–296, Jan. 2000, doi: 10.1016/S1365-1609(99)00106-9.

[33] R. P. Tiwari and K. S. Rao, “Post failure behaviour of a rock mass under the influence of triaxial and true triaxial confinement,” *Eng. Geol.*, vol. 84, no. 3–4, pp. 112–129, May 2006, doi: 10.1016/J.ENGGEO.2006.01.001.

[34] R. P. Tiwari and K. S. Rao, “Response of an Anisotropic Rock Mass under Polyaxial Stress State,” *J. Mater. Civ. Eng.*, vol. 19, no. 5, 2007, doi: 10.1061/(asce)0899-1561(2007)19:5(393).

[35] H. Oku, B. Haimson, and S. R. Song, “True triaxial strength and deformability of the siltstone overlying the Chelungpu fault (Chi-Chi earthquake), Taiwan,” *Geophys. Res. Lett.*, vol. 34, no. 9, 2007, doi: 10.1029/2007GL029601.

[36] H. Lee and B. C. Haimson, “True triaxial strength, deformability, and brittle failure of granodiorite from the San Andreas Fault Observatory at Depth,” *Int. J. Rock Mech. Min. Sci.*, vol. 48, no. 7, pp. 1199–1207, Oct. 2011, doi: 10.1016/J.IJRMMS.2011.08.003.

[37] T. Sriapai, C. Walsri, and K. Fuenkajorn, “True-triaxial compressive strength of Maha Sarakham salt,” *Int. J. Rock Mech. Min. Sci.*, vol. 61, pp. 256–265, Jul. 2013, doi: 10.1016/J.IJRMMS.2013.03.010.

[38] X. Ma and B. C. Haimson, “Failure characteristics of two porous sandstones subjected to true triaxial stresses,” *J. Geophys. Res. Solid Earth*, vol. 121, no. 9, 2016, doi: 10.1002/2016JB012979.

[39] J. F. Labuz and A. Zang, “Mohr-Coulomb failure criterion,” *Rock Mech. Rock Eng.*, vol. 45, no. 6, 2012, doi: 10.1007/s00603-012-0281-7.

[40] Yudhbir, W. Lemanza, and F. Prinzl, “An empirical failure criterion for rock masses.,” *Proc. 5th Congr. Int. Soc. Rock Mech. Melbourne, 1983. Vol.1*, 1983.

[41] M. H. Yu, Y. W. Zan, J. Zhao, and M. Yoshimine, “A Unified Strength criterion for rock material,” *Int. J. Rock Mech. Min. Sci.*, vol. 39, no. 8, pp. 975–989, Dec. 2002, doi: 10.1016/S1365-1609(02)00097-7.

[42] B. C. Haimson, “The hydrofracturing stress measuring method and recent field results,” *Int. J. Rock Mech. Min. Sci. Geomech. Abstr.*, vol. 15, no. 4, pp. 167–178, Aug. 1978, doi: 10.1016/0148-9062(78)91223-8.

[43] E. Kabwe, “Confining stress effect on the elastoplastic ground reaction considering the Lode angle dependence,” *Int. J. Min. Sci. Technol.*, vol. 30, no. 3, pp. 431–440, May 2020, doi: 10.1016/J.IJMST.2020.04.002.

[44] X. T. Feng, X. Zhang, R. Kong, and G. Wang, “A Novel Mogi Type True Triaxial Testing Apparatus and Its Use to Obtain Complete Stress–Strain Curves of Hard Rocks,” *Rock Mech. Rock Eng.*, vol. 49, no. 5, 2016, doi: 10.1007/s00603-015-0875-y.

[45] K. Mogi, “Fracture and flow of rocks under high triaxial compression,” *J. Geophys. Res.*, vol. 76, no. 5, pp. 1255–1269, Feb. 1971, doi: 10.1029/JB076i005p01255.

[46] K. Mogi, *Experimental Rock Mechanics*. 2006. doi: 10.1201/9780203964446.

[47] C. Chang and B. Haimson, “A failure criterion for rocks based on true triaxial testing,” *Rock Mech. Rock Eng.*, vol. 45, no. 6, 2012, doi: 10.1007/s00603-012-0280-8.

[48] R. K. Verma and S. Chandra, “Polyaxial strength criterion and closed-form solution for squeezing rock conditions,” *J. Rock Mech. Geotech. Eng.*, vol. 12, no. 3, pp. 507–515, Jun. 2020, doi: 10.1016/J.JRMGE.2019.06.011.

[49] D. Scussel and S. Chandra, “A new approach to obtain tunnel support pressure for polyaxial state of stress,” *Tunn. Undergr. Sp. Technol.*, vol. 36, pp. 80–88, Jun. 2013, doi: 10.1016/J.TUST.2013.01.006.

[50] S. Priest, “Three-dimensional failure criteria based on the hoek-brown criterion,” *Rock Mech. Rock Eng.*, vol. 45, no. 6, 2012, doi: 10.1007/s00603-012-0277-3.

[51] M. Singh and B. Singh, “Modified Mohr–Coulomb criterion for non-linear triaxial and polyaxial strength of jointed rocks,” *Int. J. Rock Mech. Min. Sci.*, vol. 51, pp. 43–52, Apr. 2012, doi: 10.1016/J.IJRMMS.2011.12.007.

[52] M. Singh, A. Raj, and B. Singh, “Modified Mohr–Coulomb criterion for non-linear triaxial and polyaxial strength of intact rocks,” *Int. J. Rock Mech. Min. Sci.*, vol. 48, no. 4, pp. 546–555, Jun. 2011, doi: 10.1016/J.IJRMMS.2011.02.004.

[53] H. Jiang, X. Wang, and Y. Xie, “New strength criteria for rocks under polyaxial compression,” *Can. Geotech. J.*, vol. 48, no. 8, 2011, doi: 10.1139/t11-034.

[54] H. Rafiai, “New empirical polyaxial criterion for rock strength,” *Int. J. Rock Mech. Min. Sci.*, vol. 48, no. 6, pp. 922–931, Sep. 2011, doi: 10.1016/J.IJRMMS.2011.06.014.

[55] Q. Zhang, H. Zhu, and L. Zhang, “Modification of a generalized three-dimensional Hoek–Brown strength criterion,” *Int. J. Rock Mech. Min. Sci.*, vol. 59, pp. 80–96, Apr. 2013, doi: 10.1016/j.ijrmms.2012.12.009.

[56] A. M. Al-Ajmi and R. W. Zimmerman, “Relation between the Mogi and the Coulomb failure criteria,” *Int. J. Rock Mech. Min. Sci.*, vol. 42, no. 3, pp. 431–439, Apr. 2005, doi: 10.1016/j.ijrmms.2004.11.004.

[57] L. B. Colmenares and M. D. Zoback, “A statistical evaluation of intact rock failure criteria constrained by polyaxial test data for five different rocks,” *Int. J. Rock Mech. Min. Sci.*, vol. 39, no. 6, pp. 695–729, Sep. 2002, doi: 10.1016/S1365-1609(02)00048-5.

[58] T. Benz and R. Schwab, “A quantitative comparison of six rock failure criteria,” *Int. J. Rock Mech. Min. Sci.*, vol. 45, no. 7, pp. 1176–1186, Oct. 2008, doi: 10.1016/J.IJRMMS.2008.01.007.

[59] S. Rukhaiyar and N. K. Samadhiya, “Strength behaviour of sandstone subjected to polyaxial state of stress,” *Int. J. Min. Sci. Technol.*, vol. 27, no. 6, pp. 889–897, Nov. 2017, doi: 10.1016/J.IJMST.2017.06.022.

[60] L. e S. M Kanji, M He, *Soft Rock Mechanics and Engineering*. Springer, 2020. doi: 10.1007/978-3-030-29477-9.

[61] D. M. Potts and L. Zdravković, *Finite Element Analysis in Geotechnical Engineering: Volume two - Application*. 2001. doi: 10.1680/feaigea.27831.

[62] A. L. Muller, E. do Amaral Vargas, L. E. Vaz, and C. J. Gonçalves, “Borehole stability analysis considering spatial variability and poroelastoplasticity,” *Int. J. Rock Mech. Min. Sci.*, vol. 46, no. 1, pp. 90–96, Jan. 2009, doi: 10.1016/J.IJRMMS.2008.05.001.

[63] M. Kwaśniewski, “Recent advances in studies of the strength of rocks under true triaxial compression conditions,” *Arch. Min. Sci.*, vol. 58, no. 4, 2013, doi: 10.2478/amsc-2013-0080.

[64] S.A. Ghoreishian Amiri, S.A. Sadrnejad, H. Ghasemzadeh, " A hybrid numerical model for multiphase fluid flow in a deformable porous medium," Applied Mathematical Modelling, Volume 45, Pages 881-899, ISSN 0307-904X, https://doi.org/10.1016/j.apm.2017.01.042.

[65] H. Ghasemzadeh, "Heat and contaminant transport in unsaturated soil," International Journal of Civil Engineering. Vol. 6, No. 2, June 2008.

[66] H. Ghasemzadeh, S.A. Ghoreishian Amiri, "A hydro-mechanical elastoplastic model for unsaturated soils under isotropic loading conditions," Computers and Geotechnics, Volume 51, 2013, Pages 91-100, ISSN 0266-352X, https://doi.org/10.1016/j.compgeo.2013.02.006.